An Efficient Collision Analysis Framework Enabling Real-Time Spacecraft Self-Protect

Jordan Maxwell

Ryan Blay

David Lujan

Jordan Marshall
Scout Space Inc.

ABSTRACT

A novel spacecraft conjunction analysis methodology is presented which offers significantly enhanced accuracy and computational efficiency relative to the current state-of-the-art, enabling next-generation self protect capabilities on orbit. The method is exact for Keplerian orbits, fully analytic, and applies orbit element kinematics, providing a means of accurately propagating collision uncertainty forward in time even under linearization assumptions. The mathematical and operational frameworks for the technique are presented followed by applications including propagation of collision uncertainty. Finally, conclusions are summarized and future work is identified, including relaxation of Keplerian assumptions, application of non-singular orbit elements, and additional applications of the overall framework.

1. INTRODUCTION

The increasingly congested and contested space domain necessitates advanced conjunction analysis techniques to adapt to the dynamic space environment. Modern collision evaluation tools rely on expensive ”propagate-and-check” methods which are unsuitable for deployment on spacecraft, and space assets dependant on ground-based communications present significant risk to both commercial and government space infrastructure. This capability has become critical as time horizons for a single small object cannot be addressed quick enough due to latency between assets and ground stations. Consequently, extending this method to assess dozens or hundreds of objects becomes impractical. Without immediate on-board analysis the timely detection and avoidance of such threats become unfeasible, compromising the safety and operational efficiency of space assets. To solve this, spacecraft themselves will require more refined characterization of space objects as well as responsiveness at a multitude of ranges and timescales.

Current state-of-the-art collision analysis tools utilized by multiple space agencies, such as ESA, DLR, JAXA, NASA, CNES, and CSA, follow a common operational process [7]. These steps include filtering out objects that cannot lead to collisions, propagation of spacecraft positions and covariances, calculating collision probabilities, and further investigation of high-interest events that exceed defined risk thresholds.

Initial filtering techniques, such as apogee-perigee filters, radial distance filters, and phase filters [4] [6], are applied before further categorizing the likelihood of collision. Catalogued objects that do not intersect based on these filters are immediately discarded. Once deemed a possible conjunction, these spacecraft positions and their uncertainties are propagated forward and then assessed through threshold miss distances. Either complex 3D volumetric or 2D area integrals are solved based on the encounter duration to assess either an exclusion volume or the probability of collision [3].

Beyond state-of-the-art approaches lies next-generation strategies which combine advanced computational approaches and modeling techniques to push the envelope of performance and accuracy. Surrogate models, adaptive multilevel splitting [2], analytical collision probability models [5], point process theory, and ergodic theory [1] are all recent investigations into streamlining conjunction analysis and collision avoidance procedures.

These existing and next-generation techniques remain valid for a majority of space operations, however as the growth of space traffic increases and collision timescales shrink the need for on-board autonomy will make previous methods obsolete. Having to propagate multiple resident space objects over long periods of time will no longer be feasible, and a rapid, fully-analytic solution will fulfill this need.

2. METHODOLOGY

The novel technique presented assesses potential in-space collisions with two separate analysis. First, the true anomalies at which two objects' position vectors are parallel are calculated (henceforth referred to as the conjunction condition), then the instantaneous orbital radii at these points are compared to identify whether a collision will occur. Kepler's first law states that any orbit about a single celestial body must have one of the foci at the center-of-mass of the body. An obvious consequence of this law is that all orbits about the body must share at least two points where the position vectors are parallel (two points for general orbits and infinitely-many for coplanar orbits). In general, the full collision condition can be written as

$$^{\mathscr{N}}\boldsymbol{r}_o(t^*) = {}^{\mathscr{N}}\boldsymbol{r}_c(t^*) \tag{1}$$

where $^{\mathscr{N}}\boldsymbol{r}$ is the position vector expressed in the inertial frame (designated by $\mathscr{N}$), t^* is the collision time, and the 'o' and 'c' subscripts refer to the observer and collider, respectively. Notably, these latter designations are largely semantic, as both objects are involved in the collision. A key insight facilitating the derivation of the novel collision analysis technique is to represent the position vectors in Eq. 1 as a magnitude and a direction. By doing so, this single constraint can be rewritten.

$$^{\mathscr{N}}\hat{\boldsymbol{r}}_o(t^*) = {}^{\mathscr{N}}\hat{\boldsymbol{r}}_c(t^*)\ ,\ r_o(t^*) = r_c(t^*) \tag{2}$$

Here, $^{\mathscr{N}}\hat{\boldsymbol{r}}$ indicates the instantaneous position unit vector and r the magnitude. The primary challenge in identifying collisions is determining the time at which these conditions are satisfied, motivating the propagate-and-check strategy applied in modern techniques. However, the periodicity exhibited by Keplerian orbits offers an alternative means of identifying collision locations and time horizons, with the orbit true anomaly already established as a proxy for time. The problem can therefore be transformed.

$$^{\mathscr{N}}\hat{\boldsymbol{r}}_o(\nu_o^*) = {}^{\mathscr{N}}\hat{\boldsymbol{r}}_c(\nu_c^*)\ ,\ r_o(\nu_o^*) = r_c(\nu_c^*) \tag{3}$$

where ν_o^* and ν_c^* are the true anomalies of the observer and collider, respectively, at t^*. Candidate values for these true anomalies can be determined by solving the following equation.

$$^{\mathscr{N}}\hat{\boldsymbol{r}}_o = {}^{\mathscr{N}}\hat{\boldsymbol{r}}_c \tag{4}$$

The Perifocal Reference Frame (designated $\mathscr{P}$) provides a convenient means of expressing the inertial orbit position unit vector in terms of its Classical Orbital Elements (COEs). Note that $^{\mathscr{P}}\hat{\boldsymbol{r}} = [\cos\nu, \sin\nu, 0]^{\mathrm{T}}$.

$$^{\mathscr{N}}\hat{\boldsymbol{r}} = R_3(\Omega)R_1(i)R_3(\omega)\,{}^{\mathscr{P}}\hat{\boldsymbol{r}} \tag{5}$$

In this equation, R_j indicates a rotation matrix about the j^{th} unit vector, Ω is the Right Ascension of the Ascending Node (RAAN), i is the inclination, and ω is the Argument of Periapsis (AOP). Expanding this equation and rearranging yields

$$^{\mathscr{N}}\hat{\boldsymbol{r}} = \begin{bmatrix} \cos\Omega(\cos\nu\cos\omega - \sin\nu\sin\omega) - \sin\Omega\cos i(\cos\nu\sin\omega + \sin\nu\cos\omega) \\ \sin\Omega(\cos\nu\cos\omega - \sin\nu\sin\omega) + \cos\Omega\cos i(\cos\nu\sin\omega + \sin\nu\cos\omega) \\ \sin i(\cos\nu\sin\omega + \sin\nu\cos\omega) \end{bmatrix} = \begin{bmatrix} \cos\Omega\cos u - \sin\Omega\cos i\sin u \\ \sin\Omega\cos u + \cos\Omega\cos i\sin u \\ \sin i\sin u \end{bmatrix} \tag{6}$$

where $u = \nu + \omega$ is the Argument of Latitude (AOL). Plugging this definition into Eq. 4, the upper-most equation can be solved for $\sin u_o$.

$$\sin u_o = \frac{1}{\sin\Omega_o\cos i_o}(\cos\Omega_o\cos u_o - \cos\Omega_c\cos u_c + \sin\Omega_c\cos i_c\sin u_c) \tag{7}$$

Plugging this solution into the middle equation allows for an expression for $\cos u_o$ in terms of $\Delta\Omega = \Omega_o - \Omega_c$.

$$\begin{gathered} \cos u_o = \cos u_c(\sin\Omega_o\sin\Omega_c + \cos\Omega_o\cos\Omega_c) + \cos i_c\sin u_c(\sin\Omega_o\cos\Omega_c - \cos\Omega_o\sin\Omega_c) \\ \cos u_o = \cos u_c\cos\Delta\Omega + \cos i_c\sin u_c\sin\Delta\Omega \end{gathered} \tag{8}$$

Substituting this definition back into Eq. 7 yields a similarly reduced expression.

$$\sin u_o = \frac{1}{\cos i_o}(\cos i_c\sin u_c\cos\Delta\Omega - \cos u_c\sin\Delta\Omega) \tag{9}$$

Finally, substituting the results in Eqs. 8 and 9 into the z-axis equations in Eq. 6 yields the collider true anomaly values at which the headings are parallel. As discussed previously, the distinction between the observer and collider is semantic, so the observer's true anomaly values can be calculated by simply switching the subscripts and, accordingly, the sign of $\Delta\Omega$.

$$\nu_c^* = \tan^{-1}\left(\frac{\tan i_o \sin\Delta\Omega}{\tan i_o \cos i_c \cos\Delta\Omega - \sin i_c}\right) - \omega_c \ , \ \nu_o^* = \tan^{-1}\left(\frac{\tan i_c \sin\Delta\Omega}{\sin i_o - \tan i_c \cos i_o \cos\Delta\Omega}\right) - \omega_o \tag{10}$$

Note that the addition of π to both of these values also yields angles at which Eq. 4 is satisfied. For coplanar orbits (i.e. $\Delta\Omega = 0$ and $i_c = i_o$) the conditions in Eq. 10 become singular, though the following relationship is obvious from the geometry (note that $\Delta\omega = \omega_o - \omega_c$ to maintain the previously assigned convention).

$$\nu_c^* = \nu_o + \Delta\omega \ , \ \nu_o^* = \nu_c - \Delta\omega \tag{11}$$

With solutions for the conjunction anomaly values, collisions can now be assessed through an orbit radius check at the points identified in Eqs. 10 and 11. For a given COE set, the instantaneous radius can be calculated

$$r = \frac{a(1-e^2)}{1 + e\cos\nu^*} \tag{12}$$

enabling the final collision condition to be written without explicit time dependence in terms of the orbit element sets represented as $\boldsymbol{oe} = [\boldsymbol{oe}_o^{\mathrm{T}}, \boldsymbol{oe}_c^{\mathrm{T}}]^{\mathrm{T}}$.

$$\Delta r^*(\boldsymbol{oe}) = \frac{a_o(1-e_o^2)}{1 + e_o\cos\nu_o^*} - \frac{a_c(1-e_c^2)}{1 + e_c\cos\nu_c^*} \stackrel{!}{=} 0 \tag{13}$$

The position vector of the spacecraft can be easily parameterized according to the true anomaly, but expression in terms of its mean anomaly (m) and mean motion (n) allows for linear evolution in time for Keplerian orbits. The conversion from true anomaly to mean anomaly is well known.

$$m = \tan^{-1}\left(\frac{\sqrt{1-e^2}\sin\nu}{e + \cos\nu}\right) + \pi - e\frac{\sqrt{1-e^2}\sin\nu}{1 + e\cos\nu} \tag{14}$$

Here, e is the eccentricity of the orbit. The mean motion is defined below, with a defined as the orbit Semi-Major Axis (SMA) and μ as Earth's gravity parameter.

$$n = \dot{m} = \sqrt{\frac{\mu}{a^3}} \tag{15}$$

At this stage, it's useful to introduce a new quantity here referred to as the Mean Synodic Anomaly (MSA), so-called because it goes from 0 to 2π over the synodic period between the observer and collider — the period over which the relative orbit geometries repeat. The synodic period can be calculated in terms of the mean motions.

$$P_{\mathrm{syn}} = \frac{2\pi}{\|n_o - n_c\|} \tag{16}$$

The MSA is simply the difference between the observer's and collider's mean anomalies, and the conjunction occurs when this value reaches the mean anomaly difference indicated by Eq. 10 or 11 and transformed through Eq. 14. The constant nature of each spacecraft's mean motion means that the time rate of change of the MSA is also constant. To follow convention, consider the Mean Synodyic Motion (MSM) as the denominator of Eq. 16.

$$n_{\mathrm{syn}} = \|n_o - n_c\| \tag{17}$$

The equation governing the MSA's evolution in time is analogous to that for each individual mean anomaly.

$$m_{\mathrm{syn}}(t_i) = m_{\mathrm{syn}}(t_0) + n_{\mathrm{syn}}\Delta t \tag{18}$$

The linear nature of this equation allows for a simple and efficient means to determine the time horizon to the nearest conjunction Δt^*.

$$\Delta t^*(\boldsymbol{oe}) = \frac{m_{\text{syn}}(t^*) - m_{\text{syn}}(t)}{n_{\text{syn}}} \tag{19}$$

For Keplerian orbits, the conditions above enable rapid evaluation of collision closest-miss distance and time horizon ($\sim$1 ms computation time on a standard laptop). For orbits perturbed by atmospheric drag, Solar Radiation Pressure (SRP), and non-spherical and n-body gravity, the COEs can be propagated forward in time using techniques like the well-known Gauss Planetary Equations to provide enhanced accuracy. Propagation in orbit element space is preferential to conventional techniques applying Cartesian kinematics because orbit elements are designed to evolve in a near-linear fashion even under perturbations.

In addition to enabling rapid evaluation of collision locations and times, the presented technique also facilitates transformation of uncertainty in the observer and collider COEs into uncertainty on the collision either through linearization of the conditions above or through nonlinear techniques like the Unscented Transform. While conventional techniques also permit this, the collision condition in Eq. 13 and time horizon computation in Eq. 19 provide two 1-dimensional, intuitive indicators of collision risk with far superior computational efficiency. Consider a covariance matrix $C_{\boldsymbol{oe}}$ that contains the uncertainty in the observer's and collider's COEs. This uncertainty can be transformed into a one-dimensional variance on the collision time and miss distance through linearization in the following way.

$$\sigma^2_{\Delta r^*} = \frac{\partial \Delta r^*(\boldsymbol{oe})}{\partial \boldsymbol{oe}} C_{\boldsymbol{oe}} \frac{\partial \Delta r^*(\boldsymbol{oe})}{\partial \boldsymbol{oe}}^{\mathrm{T}} \;,\; \sigma^2_{\Delta t^*} = \frac{\partial \Delta t^*(\boldsymbol{oe})}{\partial \boldsymbol{oe}} C_{\boldsymbol{oe}} \frac{\partial \Delta t^*(\boldsymbol{oe})}{\partial \boldsymbol{oe}}^{\mathrm{T}} \tag{20}$$

With the mean miss-distance and time calculated directly with Eqs. 13 and 19 and their variances provided by Eq. 20 or another technique, a Gaussian distribution can be constructed for each quantity. The collision likelihood can then be directly calculated as the value of the miss-distance distribution when $\Delta r = 0$. This is another major benefit of the presented technique. The collision likelihood in conventional strategies is calculated based on overlap between covariances projected into the collision plane, a calculation laden with both assumptions and cases where the metric poorly represents reality. The novel technique presented here directly applies probability theory and applies only the commonly-used Gaussian assumption. Additionally, the collision likelihood parameter is exactly the miss distance, which provides an intuitive way of understanding the true risk across all scenarios.

3. APPLICATIONS

Several applications of the novel technique are demonstrated in this section. Initially, a first-order comparison with existing techniques is performed, demonstrating the value of the novel technique. Next, uncertainty propagation is demonstrated using both an Unscented Kalman Filter (UKF) and Monte Carlo analysis. Finally, a geometric analysis is performed providing novel insights on impact directions and magnitudes resulting from various orbit element differences.

3.1 Comparison with Existing Techniques

Many simulations were run to demonstrate the technique. Figure 1 shows the orbit-frame location of a collider when visible to a space-based optical observer. For these simulations, only two-body gravity is applied with time steps ranging between 0.1 and 10 seconds. Two general manifolds are shown in the plot, corresponding to the two points where the orbits cross. The method discussed in the previous section is applied to generate a collision 24 hours into the simulation time. The success of the method is demonstrated by the fact that the collider goes to the origin (the collision point in the orbit-frame) at the predicted time. Notably, Figure 1 shows that many opportunities exist to observer the collider and estimate its orbit, further facilitating on-orbit self-protect capabilities.

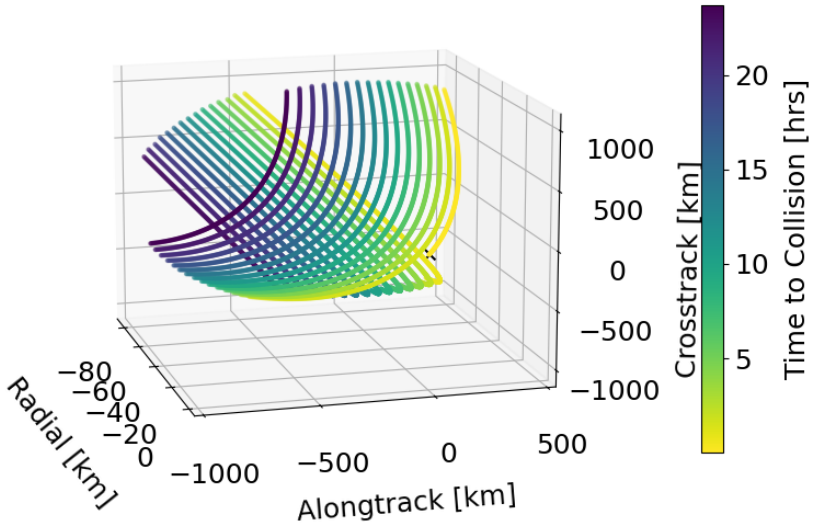

Fig. 1: Orbit frame location of collider relative to observer when measurable

Comparisons of the novel method against conventional techniques for locating collision points and times were conducted, with results shown for a variety of collision time horizons in Figure 2. Notably, the propagated solution requires a very small time step because the velocity ($\sim$ 7 km/s in Low Earth Orbit) means that distances close on sub-second time scales. For this case, the collision location and time are fairly easy to find, since only a single close fly-by occurs for each orbit. However, for orbits with very similar Semi-Major Axis (SMA), close passes occur twice per orbit for hours at a time. In this case, an even smaller simulation time step is required to precisely locate the collision — even at 1 seconds, the propagation-based strategy was sometimes off by as many as 20 orbits. By contrast, the novel technique presented here precisely locates collisions from the best estimate of two objects' COEs with negligible computational effort.

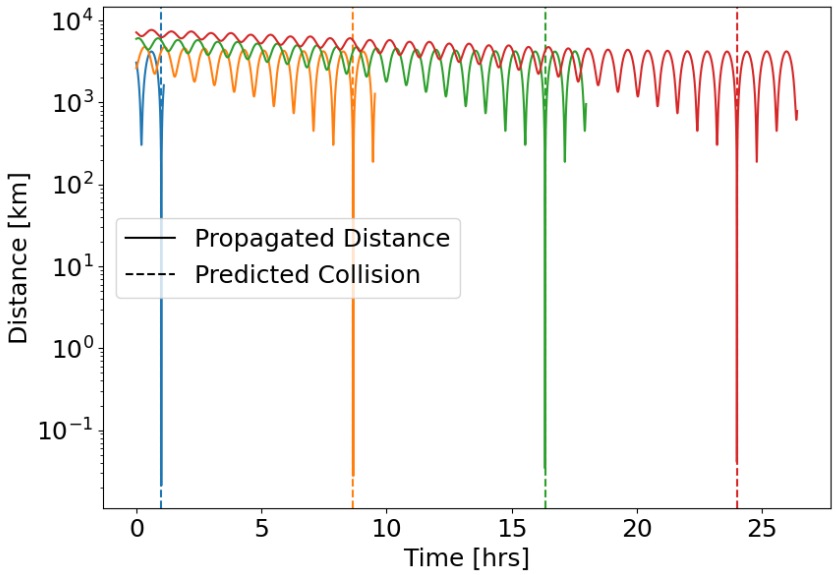

Fig. 2: Propagated distance between two colliders and predicted collision locations.

Figure 3 shows the improvement in efficiency for various collision tie horizons. Note that, for accurately predict a col-

lision, the novel technique has computation >10,000 times faster than the propagation-based technique. Application of the SGP4 model or similar analytical state prediction techniques may improve on the simulation times compared to propagation-based techniques. However, the simply dynamics formulation applied in this study is highly-efficient for propagation.

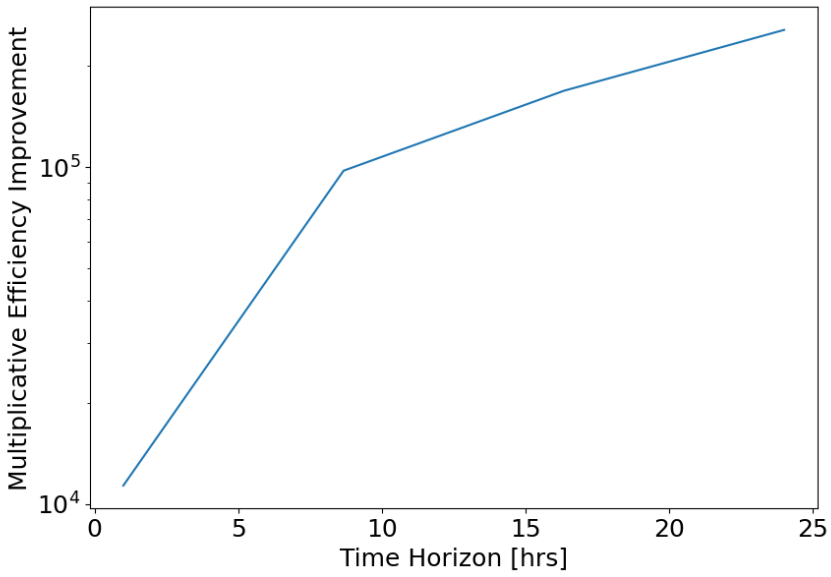

Fig. 3: Efficiency factor of novel technique relative to propagation-based strategies to achieve the same accuracy.

Future work will perform direct comparisons in evaluating collision likelihood between the novel strategy presented above and conventional techniques.

3.2 Propagating Collisions under Uncertainty

With unmodeled perturbations and imprecise measurements, any application of this collision avoidance method requires an analysis of uncertainty propagation. Understanding how the uncertainty grows and is best represented is necessary for accurate screening of potential conjunctions. The goal is to have the collision estimate stable through time and the uncertainty growth resemble as close to a Gaussian distribution as possible. This enables the extension of the Keplerian-only case and the prediction of collisions farther into the future.

To take a relevant look at the uncertainty propagation of the collision prediction, the prediction step of a UKF is used with the two colliding spacecraft's orbit elements as the state. The standard unscented transform is used to generate sigma points which are then propagated with Gauss's Planetary Equations. The state and covariance are then combined with the standard weighted summations. This is relevant because the UKF is a likely on-board filter, and if the sigma points maintain stable uncertainty growth, then this approach is feasible for autonomous collision avoidance.

In order to examine the uncertainty, the first case will only use Keplerian dynamics. The radial offset miss distance and time to collision should have no perturbation. For the examples shown, two near-circular mid-inclination spacecraft are set up with a semi-major axis of 800 km. The spacecraft orbits are designed so that a collision occurs at 2 hours into the simulation. Figure 4 shows that the miss distance, and time to collision are stable. In these figures, each red line is one of the UKF's sigma points while the solid blue line is the average and the dashed blue lines are the 3σ bounds.

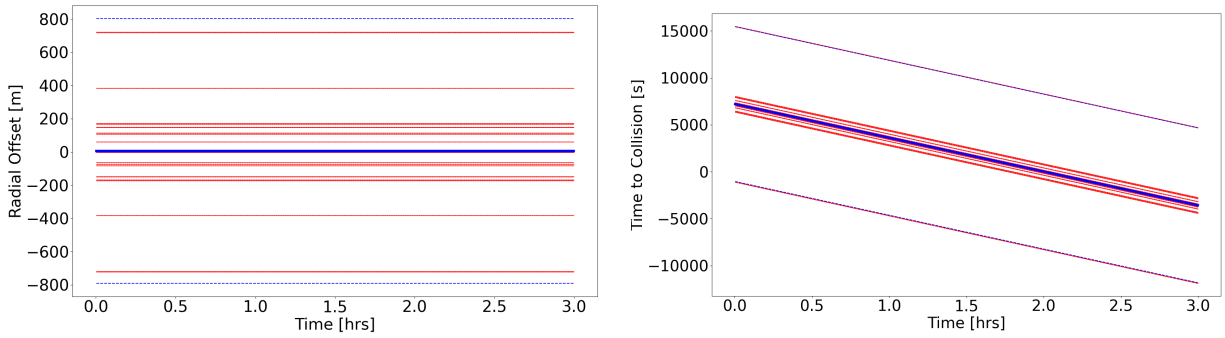

(a) Miss distance

(b) Time to collision

Fig. 4: Miss distance and time to collision between the two spacecraft for the UKF sigma points. Propagated with only Keplerian dynamics. Average given by solid blue line, and 3σ bounds in dashed blue lines.

The first clear extension of this method would be to model Earth's oblateness, captured by the J2 term in the spherical harmonics gravity model. The J2 term causes the orbit to osculate about a mean orbit while also causing secular drift of the RAAN and argument of perigee. This secular drift in orbit element coordinates further points to the advantage of the propagation in orbit elements. The uncertainty propagation will benefit from the linearity as opposed to the Cartesian state.

While J2 is one of the largest effects on satellite orbits, the other main perturbations of drag, SRP, higher-level gravity, and third-body gravity can also use Gauss Planetary Equations to propagate the orbit elements. Unlike the J2 effect, drag is hard to model accurately. Density is highly variable and often satellite ballistic coefficient modeling is imprecise. However, the orbit elements have the added benefit of effectively capturing drag uncertainty using the true anomaly and semi-major axis.

In order to handle the J2 perturbation, a couple necessary adjustments were applied. First, the osculating orbit elements were converted to mean orbital elements using the well-known Brouwer-Lyddane conversion. Next, an iterative solver was used to take account of the RAAN and apsidal precession. The initial guess is calculated using the standard formulas, and then the predicted time to collision is multiplied by the precession formulas for the RAAN and argument of perigee for both spacecraft. This process is then iterated with the improved orbit elements until the predicted collision true anomaly converges.

This example is propagated with J2 but with the same orbits defined for the Keplerian case. First, plots are shown of the miss distance and time to collision with no adjustments to see the impact of the J2 perturbation:

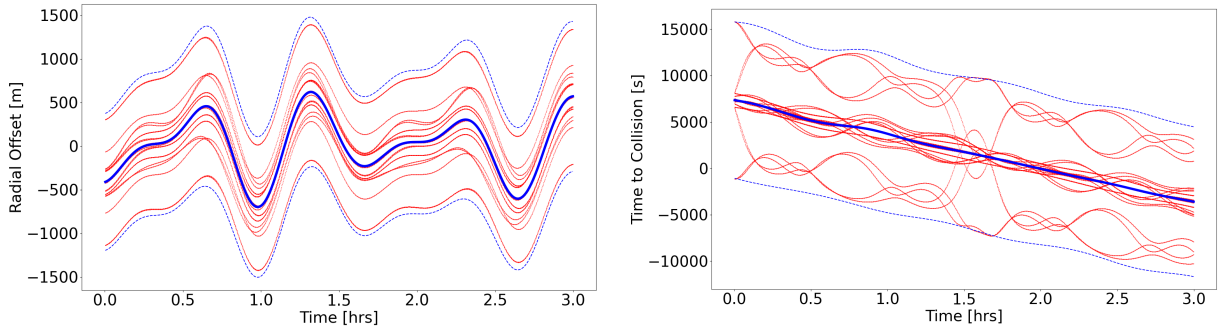

(a) Miss distance

(b) Time to collision

Fig. 5: Miss distance and time to collision between the two spacecraft for the UKF sigma points. Propagated with the J2 perturbation included, but with no adjustments to the method. Average given by solid blue line, and 3σ bounds in dashed blue lines.

It is clear from the miss distance that the J2 perturbation causes large variation that would be unhelpful during collision prediction. In Figure 6, the true anomalies of collision are shown for both spacecraft (one denoted ”self” and the other ”collider”). The top row is without any adjustments, the middle with the conversion of osculating to mean, and the bottom also including the RAAN and apsidal precession.

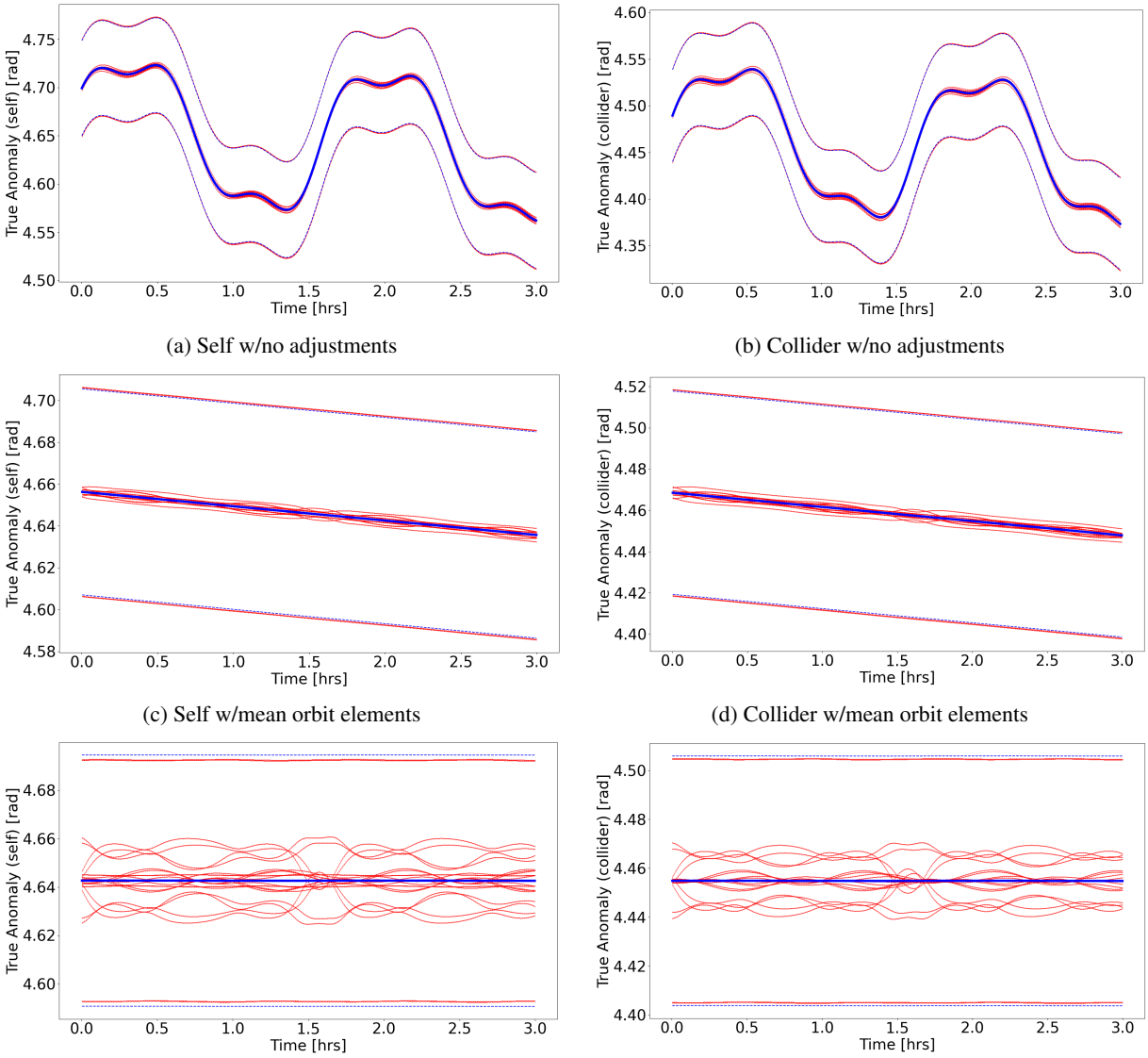

(a) Self w/no adjustments

(b) Collider w/no adjustments

(c) Self w/mean orbit elements

(d) Collider w/mean orbit elements

(e) Self w/all adjustments

(f) Collider w/all adjustments

Fig. 6: True anomalies of collision for the spacecraft. Average given by solid blue line, and 3σ bounds in dashed blue lines.

The mean orbit elements solve most of the variations, but precession drift causes error over time. This is accounted for as described above, enabling the tool to be used to accurately predict future collisions. Looking at the resulting stable miss distance and the time to collision confirm this in Figure 7. In future work, other perturbations will be accounted for in a similar way.

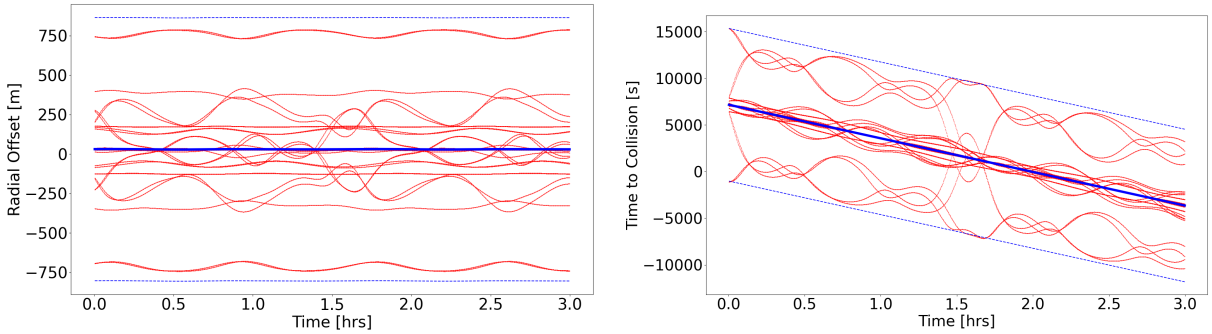

(a) Miss distance

(b) Time to collision

Fig. 7: Miss distance and time to collision between the two spacecraft for the UKF sigma points. Propagated with the J2 perturbation included, and with the appropriate method adjustments. Average given by solid blue line, and 3σ bounds in dashed blue lines.

Solving the stability issue caused by the J2 perturbation, the main question remaining is if the Gaussian assumption inherent to the unscented transform is valid, thus allowing the use of the UKF. A Monte Carlo method was chosen to confirm that these assumptions hold.

Monte Carlo (MC) methods have the advantage of approximating the true posteriori probability density function (PDF), serving as the gold standard in uncertainty quantification. However, Monte Carlo methods come with the disadvantage of needing possibly many sample points to capture an accurate representation of the posteriori PDF, thereby incurring a large computational cost. It is desirable to seek out efficient methods to capture the posteriori accurately, while not suffering from a high computational cost, in order to leverage the speed of the novel analytic collision analysis approach derived here. To that end, a comparison is made between the UKF-derived uncertainty and the uncertainty from a Monte Carlo analysis with 10,000 sample points drawn from the same Gaussian a-priori. The comparison allows for the validation and justification of using the efficient unscented transform approximation as opposed to performing a costly Monte Carlo analysis for each conjunction.

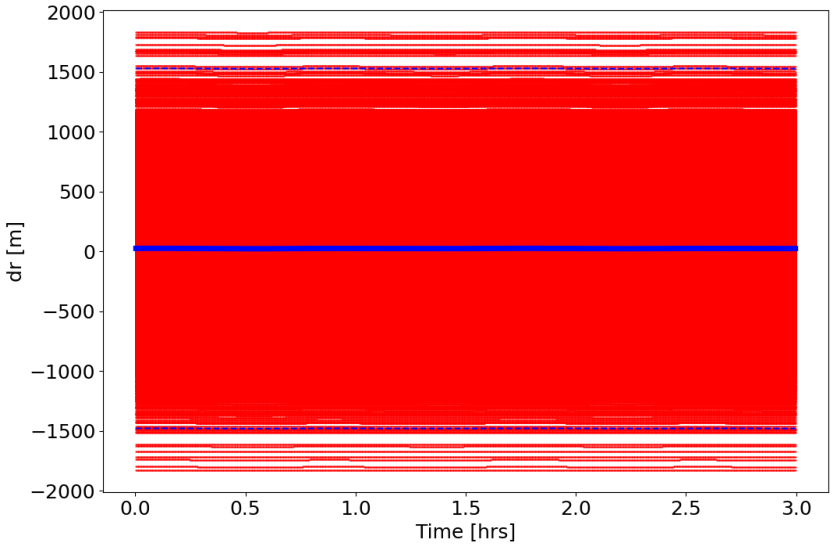

Fig. 8: Predicted radial separation between the two spacecraft at impact for each Monte Carlo sample. Average given by solid blue line, and 3σ bounds in dashed blue lines.

A set of analyses were conducted applying the J2 corrections discussed above. The predicted radial separation between

the two colliders at the collision point as a function of time is shown in Figure 8. The solid blue line is the average across all samples while the dashed blue lines are the 3σ bounds. It is observed that this predicted value is nearly constant for each MC sample, showing accurate predictions up to and beyond the point of collision.

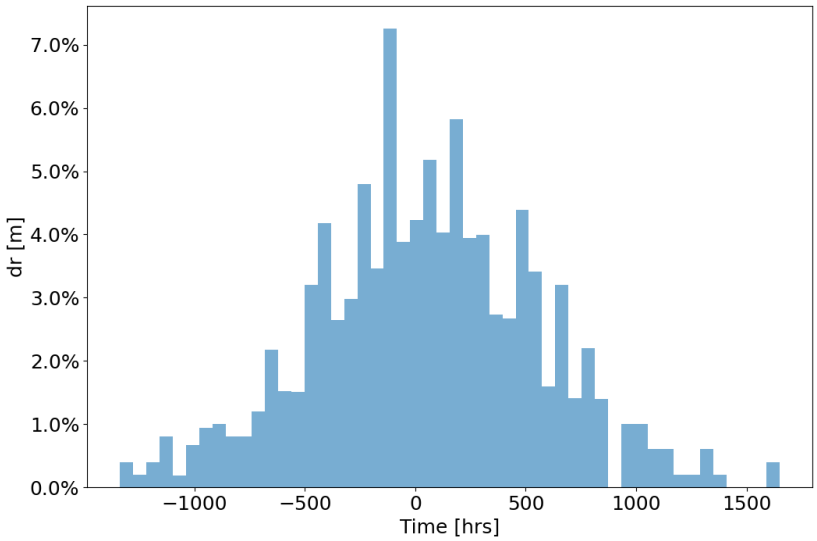

Fig. 9: Histogram of predicted radial separation at impact at each point in time between the two spacecraft for each Monte Carlo sample. Note this plot is for a scaled-down 500 sample Monte Carlo run.

Figure 9 is a histogram of the predicted radial separation between the two colliders at the collision point calculated for each time step and MC sample. Note that the histogram is for a MC trial with 500 samples, rather than 10,000. The distribution resembles a nearly Gaussian distribution with an average slightly shifted to the right. With more MC trials it is expected the distribution will be centered on 0 as it appears in Figure 8. This offset could also result from application of linearized J2 models, so future work will include further investigation.

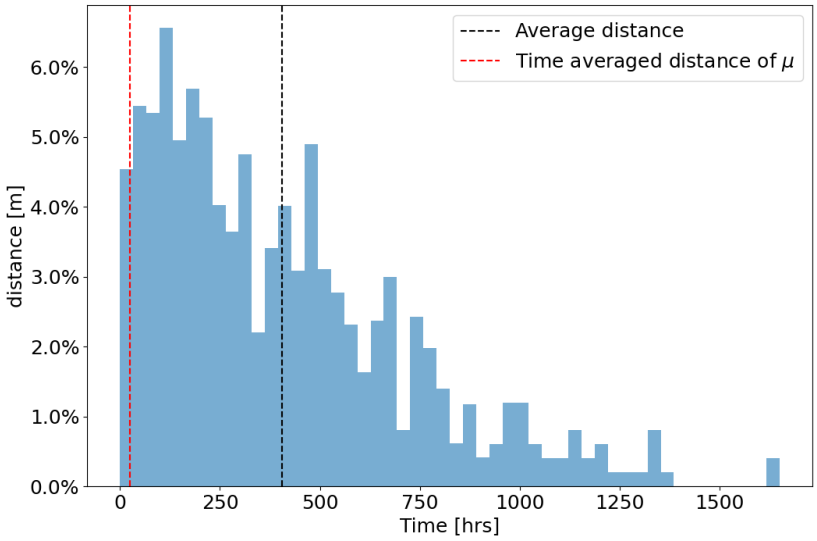

Fig. 10: Histogram of distance at each point in time between the two spacecraft for each Monte Carlo sample. Note this plot is for a scaled-down 500 sample Monte Carlo run.

Figure 10 is a histogram of the predicted distance at impact between the two colliders at each time step and MC

sample. Due to the non-negativity of the distance function, a Gaussian distribution is not recovered, however the square of a Gaussian distribution is expected. The average value of this type of distribution is equal to the variance of the underlying Gaussian. The average distance is observed to be approximately located where the variance would be if the distribution was Gaussian centered at 0. Note that this figure is also produced with 500 MC samples, rather than 10,000.

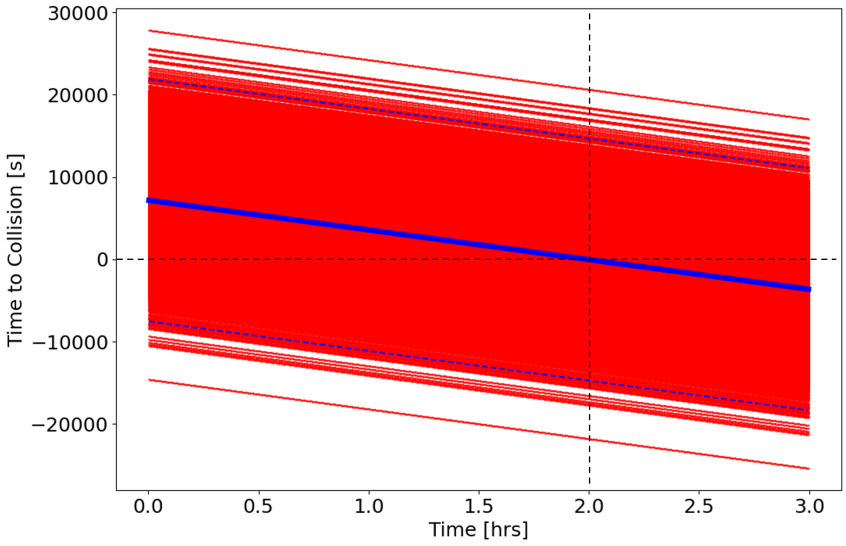

Fig. 11: Predicted time until collision between the two spacecraft for each Monte Carlo Sample. Average given by solid blue line, and 3σ bounds in dashed blue lines. The black dashed lines indicate the designed collision point.

The time history of the predicted time until collision between the colliders for each MC sample is shown in Figure 11. The solid blue line shows the average across all samples while the dashed blue lines show the 3σ bounds. The intersection between the black dashed lines show the location of where the designed collision takes place. There are a couple observations to make. First, the time to collision decreases linearly with time (as expected). Second, the average time to collision passes through the predicted collision time. Both of these observations point to the accurate prediction of the collision time even under J2 perturbations.

3.3 Collision Geometry Analysis

Another advantage of this technique is its ability to quickly analyze collision geometries to identify the most common impact headings and associated impact velocities of collider orbits. The derived knowledge supports spacecraft self-protect capabilities by informing observers which direction the most common collisions occur from, and can be easily applied to any observer craft to identify which colliders would be the most destructive. To execute this analysis, sweeps are performed varying the COEs to create conjunctions through calculation of the true anomaly location. From there, eccentricity is manipulated to force collisions if the spacecraft do not already collide with a condition neglecting colliders with altitudes below 200km. Directional headings and impact magnitude are then saved for valid collisions. Relationships can be formed amongst orbit elements as a function of their impact velocity and further analysis can be conducted into which orbit element sets will cause the highest impacts. The observer in this scenario is selected to be in a circular, mid-inclined, zero degree right ascension orbit at 500km altitude. Equation 10 above shows that only the difference in right ascension is relevant to collisions, which is why zero degrees was selected.

Figure 12 shows the relationship between right ascension and inclination, and right ascension and argument of periapsis with their effect on the impact velocity. For right ascension and inclination these elements dictate the conjunction point and display a pattern that shows based on their relationship that highly inclined colliders with a more median right ascension value will always create a greater impact magnitude. Figure 13 shows the collider approach direction and impact count in the orbit frame. This analysis implies that the majority of collisions occur near the anti-along and (not shown) along-track direction.

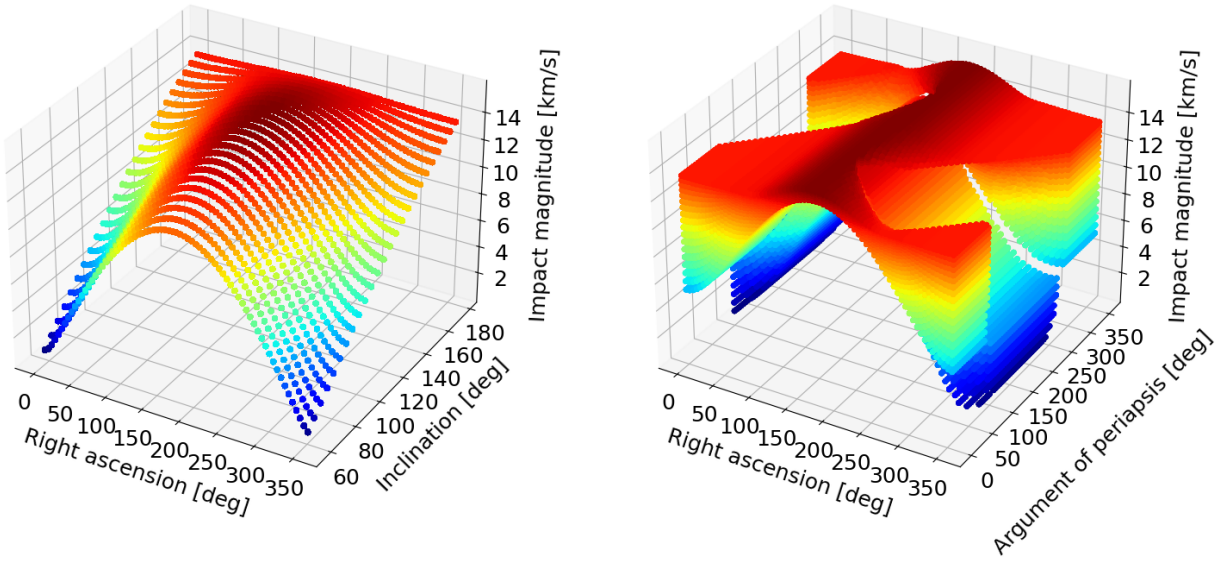

Fig. 12: Impact magnitude as a function of right ascension, inclination, and argument of periapsis.

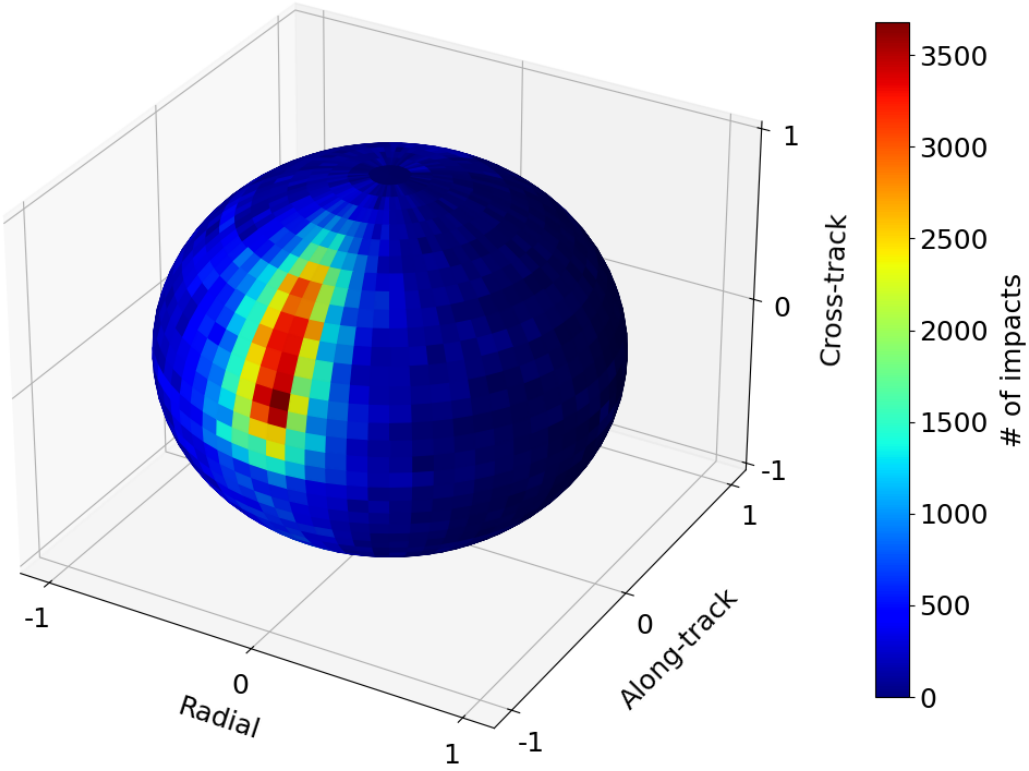

Fig. 13: Collider approach direction and impact count.

Figure 14 demonstrates the regions where high impact, low impact, and least likely impacts occur. The largest cluster of collisions occur in the positive elevation negative azimuth quadrant of the chart which agrees with the previous figure. The region with the lowest quantity of impacts is in the positive elevation positive azimuth quadrant. This figure is also showing how impact magnitude occupies each quadrant with the negative elevation and positive azimuth

region containing the lowest impact collisions.

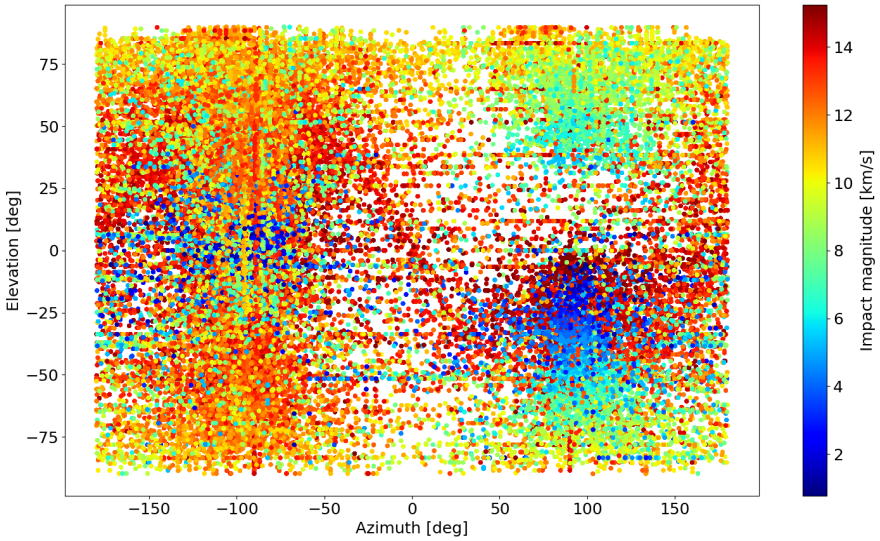

Fig. 14: Azimuth and elevation impact velocity heatmap.

4. CONCLUSIONS

A novel collision analysis technique is presented and demonstrated across various applications. The new method is shown to be far more efficiently than conventional techniques for predicting collision locations and times. An uncertainty analysis is also completed that shows the collision kinematics developed are extremely linear and can be easily modified to handle orbital perturbations. Finally, a geometric analysis is conducted to inform sensor search patterns.

Future work will focus on performing direct comparisons with existing collision likelihood analysis techniques. A more detailed perturbation analysis will also be conducted to provide accurate predictions under the influence of drag, solar radiation pressure, n-body gravity, and others. Non-singular orbit elements will also be considered to provide a more robust means of estimating both collider orbits and their potential collisions.

This work was partially supported under Phase I Small Business Innovative Research grant #FA864924P0930.

5. REFERENCES

[1] Y. Delande E. Carpine, M. Paul and V. Ruch. Point process formulation of long-term collision risk statistics from orbital fragmentation. *Journal of Guidance, Control, and Dynamics*, 47(7):1309–1326, 2024.

[2] M. Miguez J. Garcia, Y. Rivo and G. Escribano. *Novel method for the Computation of In-Orbit Collision Probability by Multilevel Splitting and Surrogate Modelling*. AIAA, 2024.

[3] Emma Kerr and N. Sánchez Ortiz. State of the art and future needs in conjunction analysis methods, processes and software. In *Proceedings of 8th European Conference on Space Debris (virtual edition, SDC8)*, pages 20–23, 2021.

[4] H. Klinkrad. One year of conjunction events of ers-1 and ers-2 with objects of the usspacecom catalog. In *2nd European Conference on Space Debris on Space Debris*, 1997.

[5] Eduardo Maria Polli, Juan Luis Gonzalo, and Camilla Colombo. Analytical model for collision probability assessments with large satellite constellations. *Advances in Space Research*, 72(7):2515–2534, 2023.

[6] Graziano M. Pina-Caballero F. Sánchez-Párez J. Kliknrad H. Sánchez-Ortiz, N. Damage: A dedicated geo debris model framework. In *3rd European Conference on Space Debris, 447–453*, 2001.

[7] F. Schiemenz, J. Utzmann, and H. Kayal. Survey of the operational state of the art in conjunction analysis. *CEAS Space Journal*, 11:255—268, 2019.